Araştırma Makalesi / Research Article

Analysis of Elastic Scattering Angular Distributions of Proton Halo Nuclei by Using Density-Dependent and Density-Independent Proximity Potentials

Murat AYGÜN*

Bitlis Eren University, Physics Department, Bitlis
(ORCID: 0000-0002-4276-3511)

Abstract
In this work, alternative potentials were sought to clarify the elastic scattering angular distributions of 1p halo nuclei ^{8}B, ^{17}F and 2p halo nucleus ^{9}C. Thirteen different versions of density-independent proximity potentials were first studied. The theoretical results were compared with each other and with experimental data, and good agreement results were obtained. Then, the calculations were repeated for density-dependent proximity potential in order to make a comparative study. It was seen that the results with density-dependent potential were not very enough in explaining the elastic scattering cross-sections of 1p and 2p halo nuclei.

Keywords: Halo nuclei, nuclear potential, proximity potential, elastic scattering, optical model.

Yoğunluğa Bağlı ve Yoğunluktan Bağımsız Proximity Potansiyeller Kullanılarak Proton Halo Çekirdeklerin Elastik Saçılma Açısal Dağılımlarının Analizi

Öz
Bu çalışmada, 1p halo çekirdekleri ^{8}B, ^{17}F ile 2p halo çekirdeği ^{9}C'un elastik saçılma açısal dağılımlarını açıklamak için alternatif potansiyeller araştırıldı. İlk olarak, yoğunluktan bağımsız proximity potansiyellerin on üç farklı versiyonu çalışıldı. Teorik sonuçlar birbirleriyle ve deneysel verilerle karşılaştırıldı ve iyi uyumlu sonuçlar elde edildi. Daha sonra, karşılaştırmalı bir çalışma yapmak için yoğunluğa bağlı proximity potansiyel için hesaplamalar tekrar edildi. Yoğunluğa bağlı potansiyel sonuçlarının 1p ve 2p halo çekirdeklerinin elastik saçılma tesir kesitlerini açıklamada çok yeterli olmadığı görüldü.

Anahtar kelimeler: Halo çekirdekler, nükleer potansiyel, proximity potansiyel, elastik saçılma, optik model.

1. Introduction

Elastic scattering is one of the most common reactions used in obtaining reliable information regarding nuclear structure and nuclear reactions. It can also be evaluated to get information about reaction observability. As a result of this, a lot of theoretical and experimental studies have been performed up to now.

The nuclear potential assumed in the description of the elastic scattering cross-sections (ESCCs) has a great importance. In this paper, different nuclear potentials such as Woods-Saxon (WS), Woods-Saxon square (WS^2), São Paulo (SP) and Double Folding (DF) can be used. However, identifying alternative potentials for the analysis of nuclear interactions remains important for nuclear reactions.

Proximity type potentials play a significant role in nuclear physics researches. They are extensively used to explain nuclear fusion reactions, α-decay and radioactivity [1-4]. Recently, Aygun has applied proximity potentials in clarifying the cross-sections of some nuclear scattering reactions [5-8]. He has obtained good agreement results with the experimental data.

*Corresponding author: maygun@beu.edu.tr
Received:21.01.2021, Accepted: 21.03.2021

Halo nuclei, which are composed of a tightly bound core and one or more nucleons moving around this core, are among the hottest topics in the past few decades. Halo nuclei can be considered as neutron or proton halo nuclei. If valence nucleon(s) is neutron(s), it is named as a neutron halo nucleus, and if valence nucleon(s) consists of proton(s), it is called as a proton halo nucleus. In this context, ^{8}B and ^{17}F are 1p halo nuclei and ^{9}C is 2p halo nucleus. Proximity potentials have been not sufficiently utilized in the analysis of ESCCs of proton halo nuclei although some reactions of neutron halo nuclei are investigated. Therefore, we think it would be useful to determine the applicability of density-dependent and density-independent proximity potentials in the analysis of the ESCCs of various proton halo nuclei.

In the present study, we investigated the elastic scattering angular distributions (ESADs) of 1p halo nuclei ^{8}B, ^{17}F and 2p halo nucleus ^{9}C by different targets. With this goal, we used thirteen versions of density-independent proximity potentials including the Proximity 1977 (Prox 77) [9], Modified Proximity 1988 (Mod-Prox 88) [10], Proximity 1995 (Prox 95) [11], Proximity 2003 (Prox 2003) [12], Proximity 2010 (Prox 2010) [13], Broglia and Winther 1991 (BW 91) [14], Aage Winther (AW 95) [15], Akyuz-Winther (AW) [16], Christensen and Winther 1976 (CW 76) [17], Bass 1973 (Bass 73) [18, 19], Bass 1980 (Bass 80) [14], Ngô 1980 (Ngo) [20] and Denisov (DP) [21]. Then, we calculated the ESADs of proton halo nuclei over density-dependent proximity potential such as Guo 2013 [22] in order to perform a comparative study. We simultaneously compared the theoretical results with the experimental data. Finally, we proposed alternative potentials for the analysis of the ESCCs of proton halo nuclei ^{8}B, ^{17}F and ^{9}C.

2. Material and Methods

2.1. Calculation Process

The total interaction potential for the theoretical calculations of proton halo nuclei can be written as

$$V_{total}(r) = V_{Nucl}(r) + V_{Coul}(r) \tag{1}$$

The nuclear potential ($V_{Nucl}(r)$) consists of the real and the imaginary parts. The real potential is produced by using thirteen various density-independent and one density-dependent versions of proximity potentials. The imaginary potential is used as WS potential in the following form

$$W(r) = \frac{W_0}{\left[1+\exp(\frac{r-R_w}{a_w})\right]}, \qquad R_w = r_w(A_P^{1/3} + A_T^{1/3}) \tag{2}$$

where W_0, r_w and a_w are the depth, radius and diffuseness parameters, respectively. The Coulomb potential ($V_{Coul}(r)$) is shown by [23].

$$V_{Coul}(r) = \frac{1}{4\pi\varepsilon_0}\frac{Z_P Z_T e^2}{r} \qquad r \geq R_C \tag{3}$$

$$= \frac{1}{4\pi\varepsilon_0}\frac{Z_P Z_T e^2}{2R_C}\left(3-\frac{r^2}{R_C^2}\right), \qquad r \leq R_C \tag{4}$$

$$R_c = 1.25(A_P^{1/3} + A_T^{1/3}) \tag{5}$$

The code FRESCO [24] is applied in the ESCC calculations.

2.2. Density-Independent Proximity Potentials

2.2.1. Prox 77, Mod-Prox 88, Prox 95, Prox 2003, Prox 2010

Prox 77 [9] is assumed as

$$V_N^{\text{Prox 77}}(r) = 4\pi\gamma b\left(\frac{C_pC_t}{C_p+C_t}\right)\Phi\left(\zeta=\frac{r-C_p-C_t}{b}\right)\text{ MeV}, \tag{6}$$

where

$$\gamma=\gamma_0\left[1-k_s\left(\frac{N-Z}{N+Z}\right)^2\right], \quad C_i=R_i\left[1-\left(\frac{b}{R_i}\right)^2+...\right] \tag{7}$$

$$b\approx 1\text{ fm},\ R_i=1.28A_i^{1/3}-0.76+0.8A_i^{-1/3}\text{ fm} \quad (i=p,t). \tag{8}$$

The universal function ($\Phi(\zeta)$), can be written as

$$\Phi(\zeta)=\begin{cases}-\frac{1}{2}(\zeta-2.54)^2-0.0852(\zeta-2.54)^3, & \text{for } \zeta\le 1.2511\\ -3.437\exp\left(-\frac{\zeta}{0.75}\right), & \text{for } \zeta\ge 1.2511\end{cases} \tag{9}$$

In the literature, different types of proximity potentials can be obtained. These potentials are the same as Proxy 77 potential except for γ_0 and k_s values which are presented in Table 1.

Table 1. γ_0 and k_s values of Prox 77, Mod-Prox 88, Prox 95, Prox 2003 and Prox 2010.

Potential type	γ_0 **(MeV/fm^3)**	k_s	**Ref.**
Prox 77	0.9517	1.7826	[25]
Mod-Prox-88	1.65	2.3	[10]
Prox 95	1.25284	2.345	[11]
Prox 2003	1.08948	1.9830	[12]
Prox 2010	1.460734	4.0	[13,26,27]

2.2.2. BW 91

BW 91 [14] is taken in the following form

$$V_N^{\text{BW91}}(r)=-\frac{V_0}{\left[1+\exp(\frac{r-R_0}{a})\right]}\text{ MeV}, \quad V_0=16\pi\frac{R_pR_t}{R_p+R_t}\gamma a, \quad a=0.63\text{ fm}, \tag{10}$$

where

$$R_0=R_p+R_t+0.29, \quad R_{p,t}=1.233A_{p,t}^{1/3}-0.98A_{p,t}^{-1/3}\text{ fm} \tag{11}$$

$$\gamma = 0.95\left[1-1.8\left(\frac{N_p - Z_p}{A_p}\right)\left(\frac{N_t - Z_t}{A_t}\right)\right]. \tag{12}$$

2.2.3. AW 95

AW 95 [15] is the same as BW 91 potential except for

$$a = \left[\frac{1}{1.17\left(1+0.53\left(A_p^{-1/3}+A_t^{-1/3}\right)\right)}\right] \text{ fm},\ R_0 = R_p + R_t, \qquad R_{p,t} = 1.2A_{p,t}^{\ 1/3} - 0.09 \tag{13}$$

2.2.4. AW

AW [16] can be written as

$$V_N^{AW}(r) = -65.4\frac{R_p R_t}{R_p + R_t}\exp\left(\frac{r - R_p - R_t}{d}\right) \text{ MeV}, \tag{14}$$

where

$$R_{p,t} = (1.20A_t^{1/3} - 0.35)\text{fm},\ d = \left[\frac{1}{1.16\left(1+0.48\left(A_p^{-1/3}+A_t^{-1/3}\right)\right)}\right] \text{ fm}. \tag{15}$$

2.2.5. CW 76

CW 76 [17] is taken as

$$V_N^{\text{CW 76}}(r) = -50\frac{R_p R_t}{R_p + R_t}\phi\left(\frac{r - R_p - R_t}{0.63}\right) \text{ MeV}, \tag{16}$$

where

$$R_{p,t} = 1.233A_{p,t}^{\ 1/3} - 0.978A_{p,t}^{\ -1/3} \text{ fm}. \tag{17}$$

2.2.6. Bass 73

Bass 73 [18, 19] can be formulated as

$$V_N^{\text{Bass 73}}(r) = -\frac{da_s A_1^{1/3} A_2^{1/3}}{R_{12}}\exp\left(-\frac{r - R_{12}}{d}\right) \text{ MeV}, \tag{18}$$

where

$$R_{12} = 1.07\left(A_1^{1/3} + A_2^{1/3}\right), \qquad d = 1.35 \text{ fm}, \qquad a_s = 17 \text{ MeV} \tag{19}$$

2.2.7. Bass 80

Bass 80 [14] can be written as

$$V_N^{Bass80}(s)=\left(\frac{R_pR_t}{R_p+R_t}\right)\Phi\left(s=r-R_p-R_t\right)\ \text{MeV}, \tag{20}$$

where

$$R_{p,t}=R_s\left(1-\frac{0.98}{R_s^2}\right),\qquad R_s=1.28A_{p,t}^{\ 1/3}-0.76+0.8A_{p,t}^{\ -1/3}\ \text{fm} \tag{21}$$

$$\phi(s)=\left[0.033\exp\left(\frac{s}{3.5}\right)+0.007\exp\left(\frac{s}{0.65}\right)\right]^{-1} \tag{22}$$

2.2.8. Ngo

Ngo [20] can be given in the following form

$$V_N^{Ngo}(r)=\left(\frac{C_pC_t}{C_p+C_t}\right)\Phi\left(s=r-C_p-C_t\right)\ \text{MeV}, \tag{23}$$

where

$$C_i=R_i\left[1-\left(\frac{b}{R_i}\right)^2+...\right],\qquad R_i=\frac{NR_{ni}+ZR_{pi}}{A_i}\qquad (i=p,t) \tag{24}$$

$$R_{pi}=1.28A_i^{1/3}\text{fm},\quad R_{ni}=(1.1375+1.875A_i^{-4})A_i^{-1/3}\ \text{fm} \tag{25}$$

and

$$\Phi(s)=\begin{cases}-33+5.4(s-s_0)^2, & \text{for s} < s_0,\\ -33\exp\left(-\frac{1}{5}(s-s_0)^2\right), & \text{for } s\geq s_0\\ s_0=-1.6\ \text{fm}\end{cases} \tag{26}$$

2.2.9. DP

DP [21] can be presented as

$$V_N^{\text{DP}}(r)=-1.989843\frac{R_1R_2}{R_1+R_2}\phi(r-R_1-R_2-2.65)\ \text{x}\left[1+0.003525139\left(\frac{A_1}{A_2}+\frac{A_2}{A_1}\right)^{3/2}-0.4113263\left(I_1+I_2\right)\right]\text{MeV}, \tag{27}$$

where

$$I_i = \frac{N_i - Z_i}{A_i}, \quad R_i = R_{ip}\left(1 - \frac{3.413817}{R_{ip}^2}\right) + 1.284589\left(I_i - \frac{0.4A_i}{A_i + 200}\right), \tag{28}$$

$$R_{ip} = 1.24A_i^{1/3}\left(1 + \frac{1.646}{A_i} - 0.191\left(\frac{A_i - 2Z_i}{A_i}\right)\right) \text{ fm} \qquad (i = 1, 2). \tag{29}$$

The universal function $\phi\left(s = r - R_1 - R_2 - 2.65\right)$ is assumed as

$$\phi(s) = \begin{cases} 1 - \dfrac{s}{0.7881663} + 1.229218s^2 - 0.2234277s^3 - 0.1038769s^4 - \\ \dfrac{R_1R_2}{R_1 + R_2}(0.1844935s^2 + 0.07570101s^3 + \\ \left(I_1 + I_2\right)\left(0.04470645s^2 + 0.0334687s^3\right) & (-5.65 \le s \le 0), \\ \left(1 - s^2\left(\begin{array}{l} 0.05410106\dfrac{R_1R_2}{R_1 + R_2}\exp\left(-\dfrac{s}{1.76058}\right) - \\ 0.539542\left(I_1 + I_2\right)\exp\left(-\dfrac{s}{2.424408}\right) \end{array}\right)\right)\exp\left(-\dfrac{s}{0.7881663}\right) & (s \ge 0), \end{cases} \tag{30}$$

2.3. Density-Dependent Guo 2013 Proximity Potential

Guo 2013 [22] can be expressed as

$$V_N^{Guo\ 2013}(r) = 4\pi\gamma b\left(\frac{R_pR_t}{R_p + R_t}\right)\Phi\left(\zeta\right), \tag{31}$$

where

$$b \approx 1 \text{ fm}, \quad \gamma = 0.9517\left[1 - 1.7826\left(\frac{N - Z}{A}\right)^2\right], \tag{32}$$

and

$$R_{p,t} = 1.28A_{p,t}^{\ 1/3} - 0.76 + 0.8A_{p,t}^{\ -1/3} \text{ fm}. \tag{33}$$

The universal function Φ(ζ) is accepted as

$$\Phi(\zeta) = -\frac{p_1}{\left[1 + \exp(\frac{\zeta + p_2}{p_3})\right]}, \qquad \zeta = \frac{r - R_1 - R_2}{b}, \tag{34}$$

where p_1 = -17.72, p_2 = 1.30, and p_3 = 0.854.

3. Results and Discussion

We analyzed the ESADs of 1p halo nuclei ^{8}B and ^{17}F and 2p halo nucleus ^{9}C using density-dependent and density-independent proximity potentials. For this purpose, we carried out the theoretical calculations over thirteen density independent nuclear potentials and one density-dependent nuclear potential.

The theoretical calculations based on density-dependent and density-independent proximity potentials were performed within the optical model. Proximity potentials were first acquired via FORTRAN code which was formed by us, and FRESCO cards were produced. Thus, the real potentials were achieved. Also, the changes with distance of Prox 77, Mod-Prox 88, Prox 95, Prox 2003, Prox 2010, BW 91, AW 95, AW, CW 76, Bass 73, Bass 80, Ngo and DP were displayed in Figure 1.

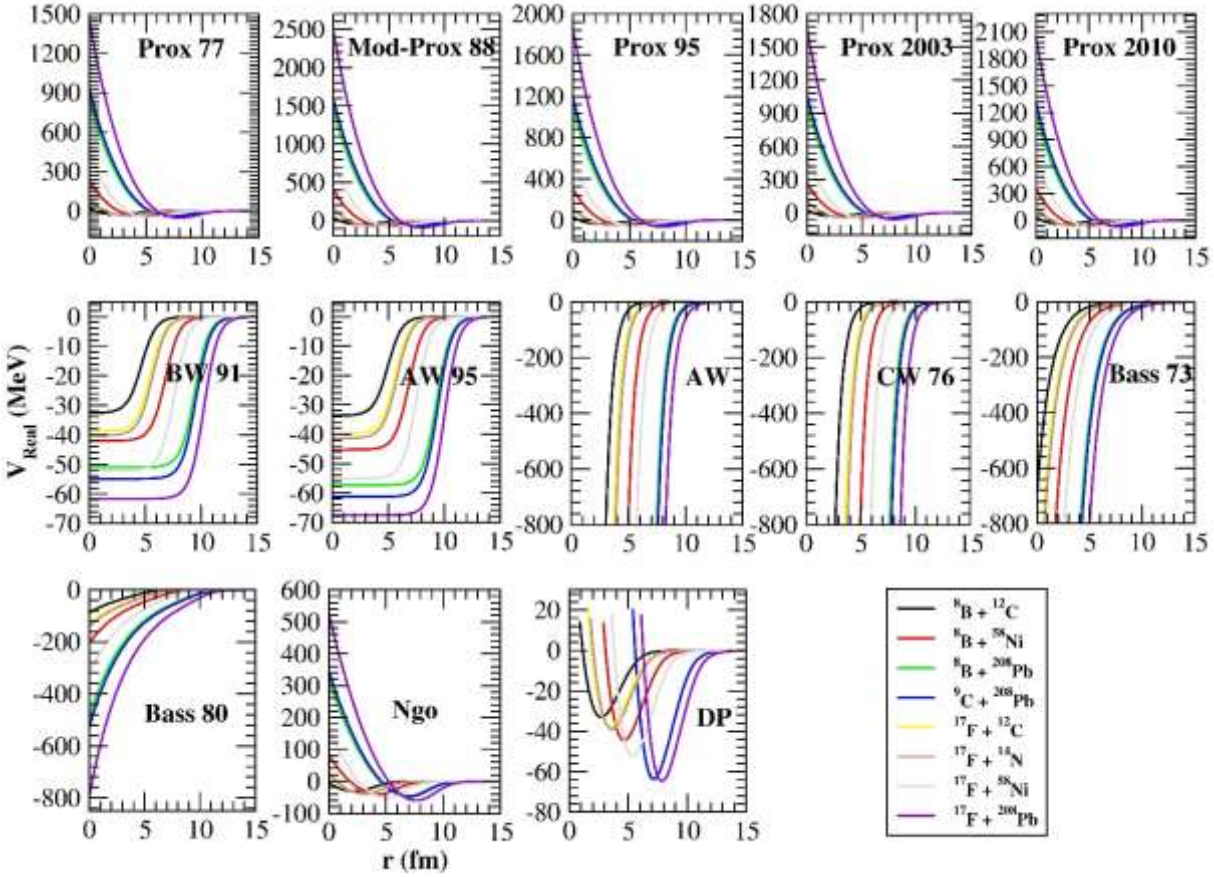

Figure 1. Changes with distance of the real potentials for Prox 77, Mod-Prox 88, Prox 95, Prox 2003, Prox 2010, BW 91, AW 95, AW, CW 76, Bass 73, Bass 80, Ngo and DP.

The WS potential for the imaginary part in all the calculations were used. The potential parameters (W_0, r_w and a_w) were released during the theoretical calculations. The r_w and a_w values were researched in steps of 0.1 fm and 0.01 fm, and the W_0 value was fixed in the results compatible with the data. The potential parameters of all the reactions analyzed in our study were listed in Tables 2, 3 and 4.

Table 2. The W_0 (in MeV), r_w (in fm) and a_w (in fm) parameters used in the elastic scattering calculations of $^{8}B + ^{12}C$, $^{8}B + ^{58}Ni$ and $^{8}B + ^{208}Pb$ reactions over Prox 77, Mod-Prox 88, Prox 95, Prox 2003, Prox 2010, BW 91, AW 95, AW, CW 76, Bass 73, Bass 80, Ngo and DP.

Reaction	Parameter	Prox 77	Mod-Prox 88	Prox 95	Prox 2003	Prox 2010	BW 91	AW 95	AW	CW 76	Bass 73	Bass 80	Ngo	DP
$^{8}B + ^{12}C$	W_0	27.0	30.0	28.0	30.0	30.0	30.0	30.0	30.0	30.0	8.50	30.0	30.0	23.0
	r_w	1.35	1.35	1.35	1.35	1.35	1.33	1.35	1.35	1.35	1.35	1.35	1.35	1.35
	a_w	0.79	0.76	0.78	0.80	0.78	0.80	0.80	0.80	0.80	0.80	0.75	0.80	0.80
$^{8}B + ^{58}Ni$	W_0	29.0	29.0	29.0	29.0	29.0	29.0	29.0	29.0	29.0	29.0	29.0	29.0	29.0
	r_w	1.44	1.43	1.44	1.44	1.44	1.46	1.44	1.44	1.44	1.44	1.44	1.44	1.49
	a_w	0.565	0.55	0.555	0.56	0.545	0.55	0.55	0.55	0.55	0.55	0.55	0.59	0.557
$^{8}B + ^{208}Pb$	W_0	38.0	38.0	38.0	38.0	38.0	35.0	38.0	38.0	38.0	28.0	38.0	42.0	43.0
	r_w	1.30	1.30	1.30	1.30	1.30	1.30	1.30	1.30	1.30	1.30	1.30	1.30	1.30
	a_w	0.75	0.74	0.75	0.75	0.75	0.75	0.75	0.75	0.75	0.62	0.74	0.75	0.75

Table 3. The same as Table 2, but for $^{17}F + ^{12}C$, $^{17}F + ^{14}N$, $^{17}F + ^{58}Ni$ and $^{17}F + ^{208}Pb$ reactions.

Reaction	Parameter	Prox 77	Mod-Prox 88	Prox 95	Prox 2003	Prox 2010	BW 91	AW 95	AW	CW 76	Bass 73	Bass 80	Ngo	DP
$^{17}F + ^{12}C$	W_0	10.0	11.0	14.0	10.2	11.7	11.8	11.0	12.0	14.0	18.0	11.5	8.00	6.30
	r_w	1.34	1.35	1.35	1.37	1.35	1.35	1.35	1.35	1.30	1.35	1.35	1.30	1.25
	a_w	0.48	0.56	0.53	0.50	0.56	0.58	0.50	0.52	0.52	0.42	0.52	0.52	0.82
$^{17}F + ^{14}N$	W_0	13.5	15.5	13.5	13.5	13.5	13.5	13.5	15.5	15.5	9.50	14.5	9.50	6.50
	r_w	1.35	1.35	1.35	1.35	1.35	1.35	1.35	1.35	1.35	1.35	1.35	1.35	1.35
	a_w	0.50	0.50	0.50	0.50	0.50	0.56	0.50	0.50	0.56	0.50	0.50	0.45	0.45
$^{17}F + ^{58}Ni$	W_0	18.0	18.0	18.0	18.0	18.0	18.0	18.0	18.0	18.0	68.0	18.0	18.0	18.0
	r_w	1.37	1.37	1.37	1.37	1.37	1.37	1.37	1.37	1.37	1.39	1.37	1.37	1.37
	a_w	0.74	0.71	0.72	0.73	0.72	0.72	0.72	0.72	0.72	0.53	0.72	0.81	0.84
$^{17}F + ^{208}Pb$	W_0	18.0	18.0	18.0	18.0	18.0	18.0	18.0	18.0	18.0	28.0	18.0	18.0	18.0
	r_w	1.37	1.33	1.37	1.37	1.37	1.34	1.37	1.37	1.34	1.20	1.32	1.37	1.37
	a_w	0.52	0.52	0.52	0.52	0.53	0.52	0.52	0.52	0.52	0.52	0.50	0.52	0.57

Table 4. The same as Table 2, but for $^{9}C + ^{208}Pb$ reaction.

Reaction	Parameter	Prox 77	Mod-Prox 88	Prox 95	Prox 2003	Prox 2010	BW 91	AW 95	AW	CW 76	Bass 73	Bass 80	Ngo	DP
$^{9}C + ^{208}Pb$	W_0	36.0	35.0	35.0	35.0	35.0	35.0	35.0	35.0	35.0	35.0	35.0	35.0	35.0
	r_w	1.31	1.27	1.27	1.27	1.27	1.27	1.27	1.27	1.27	1.27	1.27	1.27	1.35
	a_w	0.48	0.47	0.54	0.56	0.52	0.47	0.48	0.48	0.47	0.48	0.48	0.62	0.48

3.1. Analysis with Density-Independent Proximity Potentials

We first calculated the ESCCs of $^{8}B + ^{12}C$ (at 95 MeV), $^{8}B + ^{58}Ni$ (at 29.3 MeV) and $^{8}B + ^{208}Pb$ (at 164 MeV). We compared the theoretical results with the data in Figure 2. We observed that the results of the other potentials except for Bass 73 potential exhibited a very similar behavior with the data. Especially, it was seen that the result of Bass 73 potential was far from the data at 29.3 MeV. On the other hand, we can say that the proximity potentials are successful in the ^{8}B reactions.

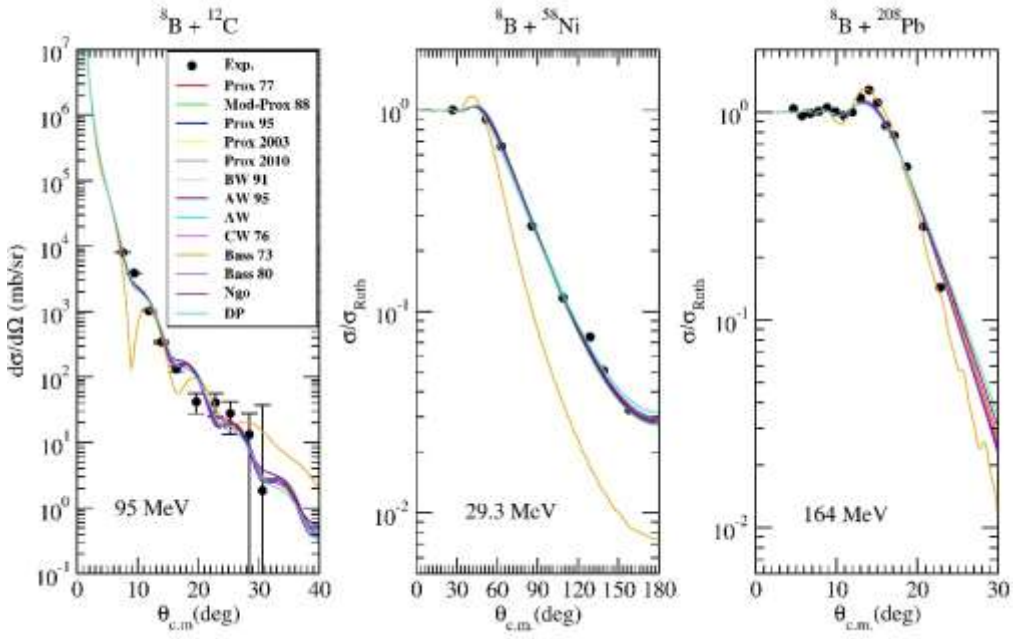

Figure 2. The ESCCs of $^{8}B + ^{12}C$, $^{8}B + ^{58}Ni$ and $^{8}B + ^{208}Pb$ reactions by using density-independent Prox 77, Mod-Prox 88, Prox 95, Prox 2003, Prox 2010, BW 91, AW 95, AW, CW 76, Bass 73, Bass 80, Ngo and DP potentials. The data are taken from Refs. [28, 29].

Then, we calculated the ESCCs of $^{17}F + ^{12}C$ (at 170 MeV), $^{17}F + ^{14}N$ (at 170 MeV), $^{17}F + ^{58}Ni$ (at 170 MeV) and $^{17}F + ^{208}Pb$ (at 170 MeV) reactions. We compared the results with the data in Figure 3. Despite the oscillatory structure of the data of $^{17}F + ^{12}C$ reaction, it can be said that the results are successful with the data. Also, the results of proximity potentials except for Bass 73 were seen to be very successful the experimental data of $^{17}F + ^{14}N$, $^{17}F + ^{58}Ni$ and $^{17}F + ^{208}Pb$ reactions.

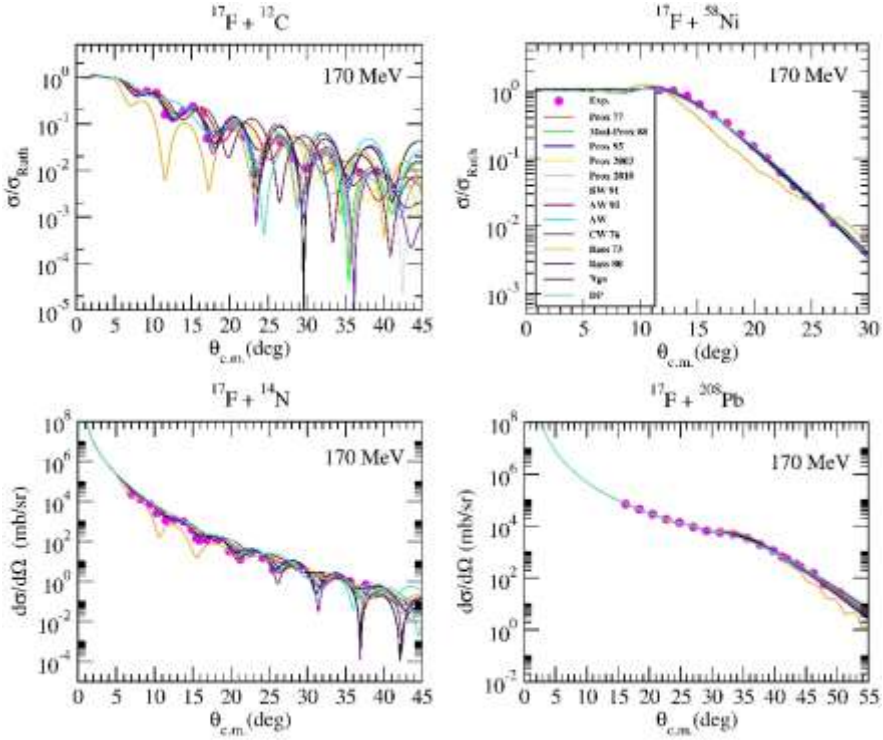

Figure 3. The same as Fig. 2, but for $^{17}F + ^{12}C$, $^{17}F + ^{14}N$, $^{17}F + ^{58}Ni$ and $^{17}F + ^{208}Pb$ reactions. The data are taken from Refs. [28, 29].

As 2p halo nucleus reaction, we examined the ESCC of $^{9}C + ^{208}Pb$ reaction at 227 MeV. We obtained the ESCCs, and compared the theoretical results and the data in Figure 4. We observed that the behaviors of the potentials except for Bass 73 potential are compatible with each other, and were found to be successful with the data. Thus, we can say that the proximity potentials except for Bass 73 would be considered as alternative potentials in explaining 2p halo nucleus reaction. Additionally, we gave the cross-section values for all the reactions analyzed over density-independent proximity potentials in Table 5. The cross-sections were observed to be supportive of each other.

Table 5. The cross-sections (in mb) calculated by using Prox 77, Mod-Prox 88, Prox 95, Prox 2003, Prox 2010, BW 91, AW 95, AW, CW 76, Bass 73, Bass 80, Ngo and DP.

Potential type	$^{8}B + ^{12}C$	$^{8}B + ^{58}Ni$	$^{8}B+^{208}Pb$	$^{17}F + ^{12}C$	$^{17}F + ^{14}N$	$^{17}F+^{58}Ni$	$^{17}F+^{208}Pb$	$^{9}C + ^{208}Pb$
Prox 77	1927	937	3664	1476	1642	2820	2632	3232
Mod-Prox 88	1921	904	3648	1633	1699	2769	2466	3035
Prox 95	1927	926	3669	1642	1654	2783	2640	3166
Prox 2003	1992	931	3666	1565	1647	2801	2636	3205
Prox 2010	1957	912	3670	1640	1661	2786	2663	3127
BW 91	1950	958	3656	1668	1737	2786	2510	3043
AW 95	2001	919	3673	1584	1680	2786	2640	3061
AW	1996	916	3672	1611	1705	2788	2646	3058
CW 76	1994	943	3672	1552	1777	2788	2514	3046
Bass 73	1570	1077	3256	1647	1654	2953	2078	3077
Bass 80	1902	920	3649	1598	1684	2788	2392	3060
Ngo	1986	971	3712	1378	1499	2965	2622	3333
DP	1873	1024	3717	1440	1366	3026	2713	3408

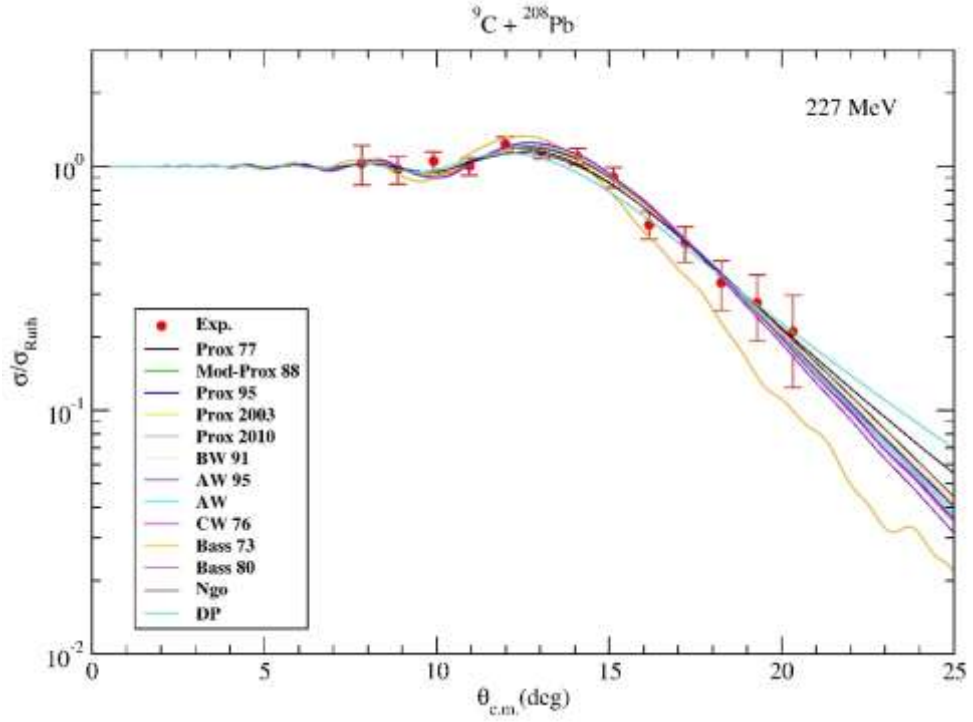

Figure 4. The same as Fig. 2, but for $^{9}C + ^{208}Pb$ reaction. The data are taken from Refs. [28, 29].

3.2. Analysis with Density-Dependent Proximity Potential

We also examined the ESAD of 1p halo nuclei ^{8}B and ^{17}F and 2p halo nucleus ^{9}C reactions by using density-dependent proximity potential which consist of Guo 2013.

We calculated the ESCCs of $^{8}B + ^{12}C$ (at 95 MeV), $^{8}B + ^{58}Ni$ (at 29.3 MeV) and $^{8}B + ^{208}Pb$ (at 164 MeV). We compared our results with the data in Figure 5. Guo 2013 potential are in very good agreement with the data of $^{8}B + ^{12}C$ and $^{8}B + ^{208}Pb$ systems, but not valid for $^{8}B + ^{58}Ni$.

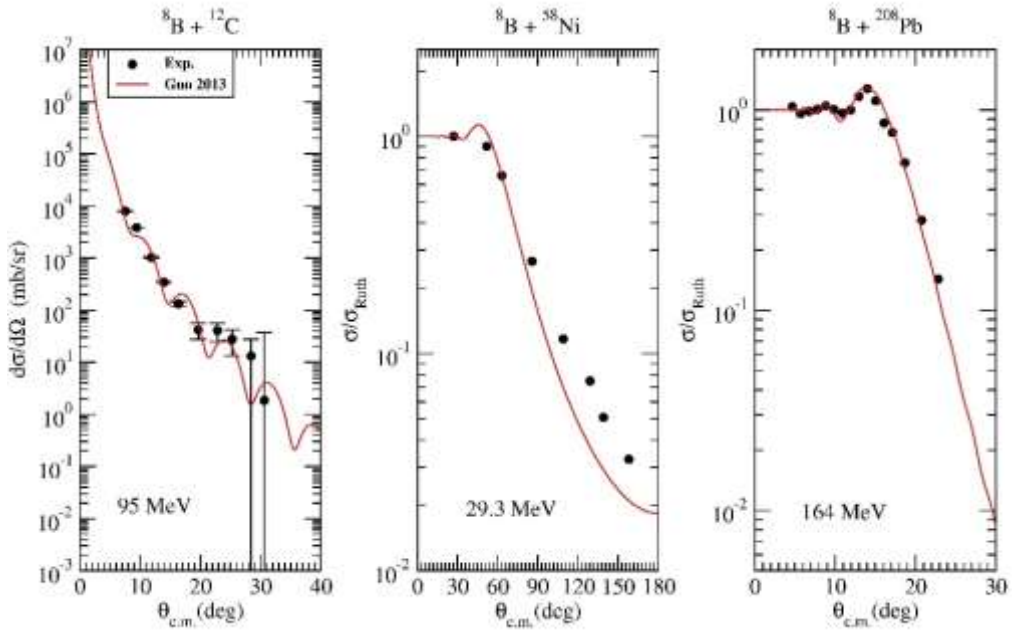

Figure 5. The ESCCs of $^{8}B + ^{12}C$, $^{8}B + ^{58}Ni$ and $^{8}B + ^{208}Pb$ reactions by using density-dependent Guo 2013 potential.

Similarly, we acquired the ESCCs of $^{17}F + ^{12}C$ (at 170 MeV), $^{17}F + ^{14}N$ (at 170 MeV), $^{17}F + ^{58}Ni$ (at 170 MeV) and $^{17}F + ^{208}Pb$ (at 170 MeV) reactions. We presented the results with the data in Figure 6. We observed that Guo 2013 potential shows an average behavior with the experimental data.

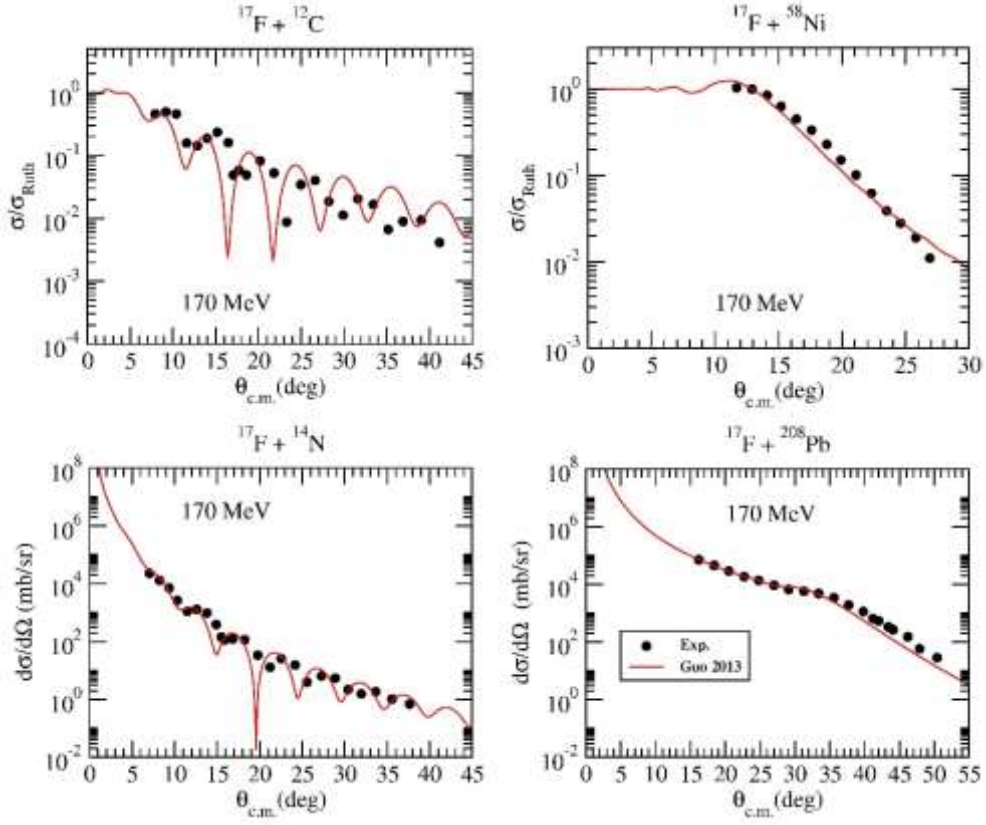

Figure 6. The same as Fig. 5, but for $^{17}F + ^{12}C$, $^{17}F + ^{14}N$, $^{17}F + ^{58}Ni$ and $^{17}F + ^{208}Pb$ reactions.

Finally, we calculated the ESCC of $^{9}C + ^{208}Pb$ reaction at 227 MeV for density-dependent version of the proximity potentials, and compared the theoretical result with the data in Figure 7. We observed that the results of Guo 2013 were not very successful with the data.

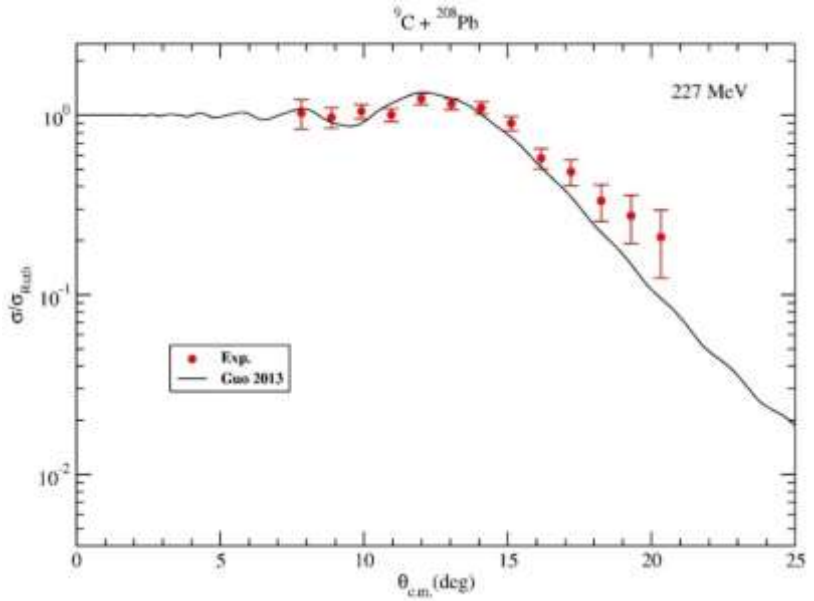

Figure 7. The same as Fig. 5, but for $^{9}C + ^{208}Pb$ reaction.

3.3. Comparison of Density-Dependent and Density-Independent Proximity Potentials

We compared the results of density-dependent and density-independent proximity potentials for $^{8}B + ^{12}C$ (at 29.3 MeV), $^{9}C + ^{208}Pb$ (at 227 MeV) and $^{17}F + ^{208}Pb$ (at 170 MeV) reactions in Figure 8 as an example. We first found that the results of density-independent proximity potentials were very successful with the ESCCs generally. On the other hand, we observed that the results of density-dependent Guo 2013 potential were not very sufficient to describe the elastic scattering data of the proton halo nucleus reactions. We can say that density-independent Prox 77 potential are more successful in explaining the experimental data of the elastic scattering of proton halo nuclei.

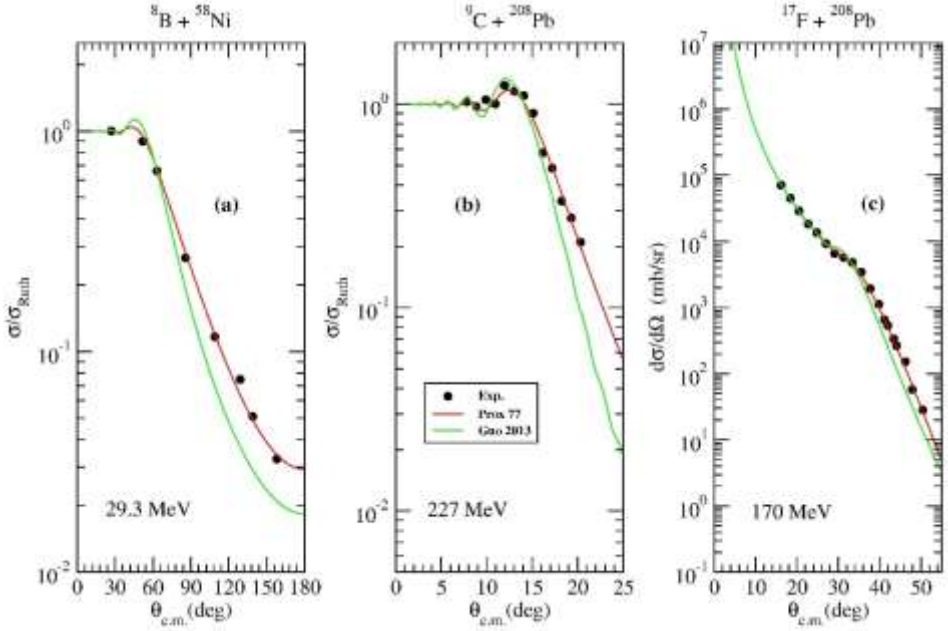

Figure 8. A comparison of the ESCCs of density-independent Prox 77 and density-dependent Guo 2013 potential for (a) $^{8}B + ^{58}Ni$, (b) $^{9}C + ^{208}Pb$ and (c) $^{17}F + ^{208}Pb$.

4. Summary and Conclusions

In this work, we tried to see the effectiveness of density-dependent and density independent proximity potentials in explaining the ESCCs of 1p and 2p halo nuclei. We obtained the ESCCs for thirteen different density-independent proximity potentials and one density-dependent proximity potential. Except for Bass 73, we noticed that results of density-independent proximity potentials are very successful in explaining the ESCCs. In this context, we can say that these potentials would be evaluated as alternative nuclear potentials for the analysis of the ESCCs of 1p and 2p halo nuclei.

In addition, we repeated the theoretical calculations for one density-dependent potential. We observed that the density-dependent Guo 2013 potential was not very enough for the analysis of the ESCCs of 1p and 2p halo nuclei. We think that Guo 2013 potential needs to be further examined as alternative potentials for the analysis of different nuclear reactions.

Author's Contributions

The author gave final approval of the current version and any revised version to be submitted to the journal.

Statement of Conflicts of Interest

No potential conflict of interest was reported by the authors.

Statement of Research and Publication Ethics

The authors declare that this study complies with Research and Publication Ethics.

References

[1] Yao Y.J., Zhang G.L., Qu W.W., Qian J.Q. 2015. Comparative studies for different proximity potentials applied to α decay. European Physical Journal A, 51:122.

[2] Ghodsi O.N., Daei-Ataollah A. 2016. Systematic study of α decay using various versions of the proximity formalism. Physical Review C, 93: 024612.

[3] Santhosh K.P., Sukumaran I. 2017. Heavy particle decay studies using different versions of nuclear potentials. European Physical Journal Plus, 132: 431.

[4] Aygun M., Aygun Z. 2019. A comprehensive analysis of ^{9}Li + ^{70}Zn fusion cross section by using proximity potentials, temperature dependent density distributions and nuclear potentials. Revista Mexicana de Física, 65: 573-582.

[5] Aygun M. 2020. A comprehensive theoretical analysis of ^{22}Ne nucleus by using different density distributions, different nuclear potentials and different cluster approach. International Journal of Modern Physics E, 29: 1950112.

[6] Aygun M. 2018. Alternative potentials analyzing the scattering cross sections of 7,9,10,11,12,14Be isotopes from a ^{12}C target: Proximity Potentials. Journal of the Korean Physical Society, 73: 1255-1262.

[7] Aygun M. 2018. A Comparison of proximity potentials in the analysis of heavy-ion elastic cross sections. Ukrainian Journal of Physics, 63: 881.

[8] Aygun M. 2018. The application of some nuclear potentials for quasielastic scattering data of the 11Li + 28Si reaction and its consequences. Turkish Journal of Physics, 42: 302-311.

[9] Blocki J., Randrup J., Swiatecki W.J., Tsang C.F. 1977. Proximity forces. Annals of Physics, 105: 427.

[10] Kumar R. 2011. Effect of isospin on the fusion reaction cross section using various nuclear proximity potentials within the Wong model. Physical Review C, 84: 044613.

[11] Moller P., Nix J.R., Myers W.D., Swiatecki W.J. 1995. Nuclear Ground-State Masses and Deformations. Atomic Data and Nuclear Data Tables, 59: 185.

[12] Pomorski K., Dudek J. 2003. Nuclear liquid-drop model and surface-curvature effects. Physical Review C, 67: 044316.
[13] Dutt I., Puri R.K. 2010. Comparison of different proximity potentials for asymmetric colliding nuclei. Physical Review C, 81: 064609.
[14] Reisdorf W. 1994. Heavy-ion reactions close to the Coulomb barrier. Journal of Physics G: Nuclear and Particle Physics, 20: 1297.
[15] Winther A. 1995. Dissipation, polarization and fluctuation in grazing heavy-ion collisions and the boundary to the chaotic regime. Nuclear Physics A, 594: 203-245.
[16] Akyüz Ö., Winter A. 1981. Proceedings of the International School of Physics Enrico Fermi, Course LXXVII, Varenna, Italy Ed. by R. A. Broglia, C. H. Dasso, and R. Richi (North-Holland, Amsterdam), p. 492.
[17] Christensen P.R., Winther A. 1976. The evidence of the ion-ion potentials from heavy ion elastic scattering. Physics Letters B, 65: 19-22.
[18] Bass R. 1973. Threshold and angular momentum limit in the complete fusion of heavy ions. Physics Letters B, 47 (1973): 139.
[19] Bass R. 1974. Fusion of heavy nuclei in a classical model. Nuclear Physics A, 231: 45.
[20] Ngô H., Ngô C. 1980. Calculation of the real part of the interaction potential between two heavy ions in the sudden approximation. Nuclear Physics A, 348: 140-156.
[21] Denisov V.Yu. 2002. Interaction potential between heavy ions. Physics Letters B, 526: 315-321.
[22] Guo C.L., Zhang G.L., Le X.Y. 2013. Study of the universal function of nuclear proximity potential from density-dependent nucleon–nucleon interaction. Nuclear Physics A, 897: 54.
[23] Satchler G.R. 1983. Direct Nuclear Reactions. Oxford University Press, Oxford.
[24] Thompson I.J. 1988. Coupled reaction channels calculations in nuclear physics. Computer Physics Reports, 7: 167.
[25] Myers W.D., Swiatecki W.J. 1966. Nuclear masses and deformations. Nuclear Physics, 81: 1-60.
[26] Dutt I., Puri R.K. 2010. Role of surface energy coefficients and nuclear surface diffuseness in the fusion of heavy-ions. Physical Review C, 81: 047601.
[27] Gharaei R., Zanganeh V., Wang N. 2018. Systematic study of proximity potentials for heavy-ion fusion cross sections. Nuclear Physics A, 979: 237-250.
[28] https://www-nds.iaea.org/exfor/ (Access date: 30.05.2021).
[29] http://nrv.jinr.ru/nrv/ (Access date: 30.05.2021).